

Outlier Suppression+: Accurate quantization of large language models by equivalent and optimal shifting and scaling

Xiuying Wei^{1, 2}, Yunchen Zhang^{2, 4}, Yuhang Li³, Xiangguo Zhang²,
Ruihao Gong², Jinyang Guo¹, Xianglong Liu^{1*}

¹State Key Lab of Software Development Environment, Beihang University

²SenseTime Research, ³Yale University

⁴University of Electronic Science and Technology of China

weixiuying966@gmail.com, yuhang.li@yale.edu, {jinyangguo, xl.liu}@buaa.edu.cn
{zhangyunchen, zhangxiangguo, gongruihao}@sensetime.com

Abstract

Quantization of transformer language models faces significant challenges due to the existence of detrimental outliers in activations. We observe that these outliers are asymmetric and concentrated in specific channels. To address this issue, we propose the Outlier Suppression+ framework. First, we introduce channel-wise shifting and scaling operations to eliminate asymmetric presentation and scale down problematic channels. We demonstrate that these operations can be seamlessly migrated into subsequent modules while maintaining equivalence. Second, we quantitatively analyze the optimal values for shifting and scaling, taking into account both the asymmetric property and quantization errors of weights in the next layer. Our lightweight framework can incur minimal performance degradation under static and standard post-training quantization settings. Comprehensive results across various tasks and models reveal that our approach achieves near-floating-point performance on both small models, such as BERT, and large language models (LLMs) including OPTs, BLOOM, and BLOOMZ at 8-bit and 6-bit settings. Furthermore, we establish a new state of the art for 4-bit BERT.

1 Introduction

Transformer language models (e.g., BERT, LLMs) have garnered significant attention due to their remarkable performance and scalable model size. These models have evolved from hundreds of millions of parameters (Devlin et al., 2018; Liu et al., 2019; Radford et al., 2018) to hundreds of billions of parameters (Brown et al., 2020; Zhang et al., 2022; Smith et al., 2022). This necessitates the employment of compression techniques (Han et al., 2015; Hinton et al., 2015; Zoph and Le, 2016; Le-Cun et al., 1989) for practical deployment. Among

these techniques, quantization (Jacob et al., 2018) has emerged as a general and primary paradigm for reducing both memory footprint and computational overhead.

However, quantization, particularly post-training quantization (PTQ) (Choukroun et al., 2019; Banner et al., 2018; Nagel et al., 2020), which operates with limited data and GPU resources, has become increasingly challenging for these models (e.g., a 12% accuracy drop in BERT (Bondarenko et al., 2021) and catastrophic degradation in OPT-175B (Dettmers et al., 2022)). This is caused by the presence of detrimental outliers in activation (e.g., the width of distribution can be 80 for BERT and even 140 for OPTs), which prevents quantization from accurately expressing floating-point numbers.

To combat the outlier bottleneck in quantization, researchers make in-depth investigations and find the concentration phenomenon that outliers typically appear in certain channels. Hence, some works (Bondarenko et al., 2021; Dettmers et al., 2022) explored various fine-grained quantization schemes to provide additional consideration for them while some (Wei et al., 2022b; Xiao et al., 2022) attempted to diminish them through a scaling operation, which can be migrated to subsequent modules to maintain floating-point (FP) equivalence. However, we find that they ignore the asymmetric property of outliers that relatively small channel ranges can result in a significantly large range for the entire tensor (e.g., as shown in Fig. 1a, a single channel on OPT-66B occupies the axis from -97 to -58 with a size of 39, but the total size can reach up to 140). In the meantime, existing work did not quantitatively analyze the effect of activation scaling on the quantization of subsequent layer's weight well.

In this paper, we propose the Outlier Suppression+ framework to suppress outliers under static and standard quantization settings. First, to eliminate asymmetric presentation and effectively deal

*Corresponding author.

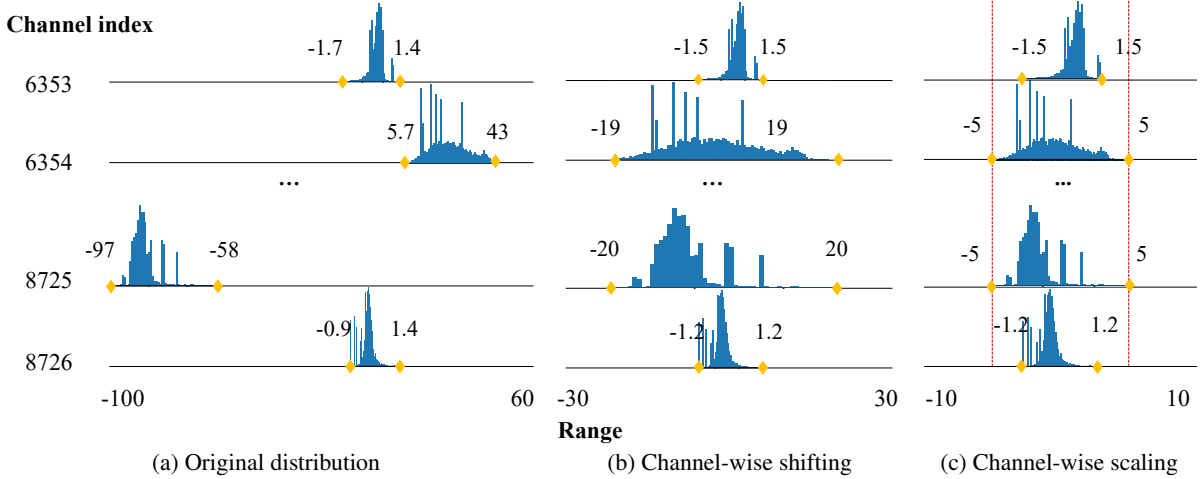


Figure 1: Distribution of OPT-66B. [Fig. 1a](#) shows the original distribution with asymmetric outliers consistently occurs at certain channels, owning considerable range (-97, 43). [Fig. 1b](#) depicts the channel-wise shifting operation to decrease the tensor range by eliminating the asymmetry. [Fig. 1c](#) further scales down the outliers to threshold 5 and finally results in a distribution ranging from -5 to 5.

with channels full of outliers, we introduce channel-wise shifting and scaling operations that adjust and scale down problematic activation signals while transferring both the reversed effects to subsequent modules for an equivalent FP network. Second, regarding finding optimal values for these operations, our proposed shifting technique can align the center of distribution across channels, making the whole tensor range determined by the maximum channel range instead of asymmetric outliers. Then, we devise reasonable scaling factors that achieve a balanced quantization burden between activation and following weights by considering their interactive results.

Our algorithm can be carried out efficiently and enjoy affordability on real hardware, producing more quantization-friendly models in minutes and requiring no extra inference burden on LLMs.

Our main contributions can be summarized in three aspects:

1. Focusing on the asymmetric attribute of outliers and their consistent emergence at specific channels, we develop channel-wise shifting and scaling operations to suppress them. To establish an equivalent FP network, we design a unified migration pattern that transfers reversed effects to succeeding modules.
2. We introduce an efficient and lightweight technique to determine optimal shifting and scaling values for more quantization-friendly models. The technique first eliminates the asymmetric exhibition and then scales down outliers with a balanced quantization burden between challeng-

ing activation and subsequent weights in terms of their interplay.

3. We assess the efficacy of our approach on both small models (BERT) and LLMs (OPTs, BLOOM, and BLOOMZ) under the PTQ background. Experimental results across a diverse range of datasets, such as the GLUE benchmark and multiple zero-shot tasks, demonstrate that our method achieves near-floating point performance in 8-bit and 6-bit cases. Notably, our approach establishes the state of the art for 4-bit BERT models with 15.5% improvement.

2 Preliminary

Basic Notations. We denote matrices as upper case letters (e.g., X) and vectors as lower case letters (e.g., x). Operator \odot and \oslash represent element-wise multiplication on matrices or vectors. We use WX as matrix-matrix multiplication. Furthermore, $X_{t,j}$ refers to the element of the t -th token and the j -th embedding or channel in transformer models. $Q(\cdot)$ denotes the quantization function.

Outlier Suppression. [Wei et al. \(2022b\)](#) describes an outlier suppression framework to suppress the notorious outliers. Observing that outliers concentrate in certain channels, a component of the framework called Gamma Migration adopts a scaling vector for scaling outliers and migrates it to later modules.

However, this approach still wastes a large portion of the quantization levels on the extreme asymmetric shape of outliers. Also, it simply utilizes the scaling parameter in LayerNorm (LN), namely

gamma, to weaken the outliers. This fixed value is not always desirable without the perception of quantization and quantitative evaluation of the migrated burden on later weight.

3 Method

In this section, we first present our equivalent shifting and scaling operations, which mitigate outliers in activation and recover equivalent FP models by updating subsequent modules. We then introduce optimal shifting and scaling factors.

3.1 Equivalent shifting and scaling

In this section, we consider the features of outliers and design shifting and scaling operations followed by a unified migration pattern.

3.1.1 Outlier shifting and scaling

Channel-wise shifting. In transformers like LLMs, outliers exhibit asymmetric behavior. Recall that in [Fig. 1a](#), the 8725-th channel displays a hard negative interval (-97, -58), while another channel dominates hard positive representations (5.7, 43). Due to this asymmetry, even if the range of each channel is relatively small, such as 40 and 38 for channels containing outliers and minuscule values for normal channels, the range of the entire tensor can swell to a considerably large value (e.g., 140, ranging from -97 to 43), which negatively affects quantization performance.

Considering the tensor range subjected by asymmetric outliers, we are motivated to eliminate the impact of asymmetry by taking the following operation:

$$\widetilde{\mathbf{X}}' = \mathbf{X} - \mathbf{z}, \quad (1)$$

where \mathbf{z} serves as a row vector ($\mathbf{z} \in \mathbb{R}^n$). The calculation of \mathbf{z} will be introduced later in [Sec. 3.2.1](#). Then, a new tensor $\widetilde{\mathbf{X}}'$ is generated by aligning centers of different channels together, contributing to a much smaller tensor range and thus better quantization performance. For instance, from [Fig. 1b](#), we can find that the distribution width has been reduced to 40 from a significant number of 140 after channel-wise shifting.

Channel-wise scaling. In addition to outliers manifesting as hard negative or positive signals, they also predominantly accumulate in specific channels over various inputs, such as the 8725-th and the 6354-th channels in [Fig. 1a](#). These channels exhibit more aggressive values than others. Therefore, after channel-wise shifting, we propose to

narrow them down to further ease the quantization difficulty via scaling factors.

$$\widetilde{\mathbf{X}} = (\mathbf{X} - \mathbf{z}) \oslash \mathbf{s}. \quad (2)$$

In the above equation, the row vector $\mathbf{s} \in \mathbb{R}^n$ would additionally shrink the shifted tensor and bring the final quantization-friendly activation $\widetilde{\mathbf{X}}$ (e.g., in [Fig. 1c](#), a tensor with a size of 10 can be acquired after scaling down the signals over 5). Optimal calculation of \mathbf{s} will be given in [Sec. 3.2.2](#).

Implementation. It is easy to implement these operations. For example, to shift and scale the output of LayerNorm, we only need to replace its linear transformation parameters β and γ with $(\beta - \mathbf{z}) \oslash \mathbf{s}$ and $\gamma \oslash \mathbf{s}$ as shown in [Fig. 2](#). For other outputs, by updating parameters in the former DeQuant function, the shifted and scaled activation can be obtained.

3.1.2 Unified migration pattern

As mentioned in [Eq. \(1\)](#) and [Eq. \(2\)](#), we subtract \mathbf{z} and divide \mathbf{s} to make the problematic activation resilient to quantization. To keep an equivalent FP model, a unified migration pattern is proposed that transfers both reversed shifting and scaling vectors to subsequent modules. We demonstrate the feasibility of this algorithm on two common structures.

Linear Layer. First, we consider a prevalent scenario where a linear (convolutional) layer immediately follows. Reversing the above operations (i.e., $(\widetilde{\mathbf{X}} \odot \mathbf{s} + \mathbf{z})\mathbf{W}^\top + \mathbf{b}$) equals to updating the $\mathbf{W} \in \mathbb{R}^{m,n}$ and $\mathbf{b} \in \mathbb{R}^m$ in the next layer, given by

$$\begin{aligned} & (\widetilde{\mathbf{X}} \odot \mathbf{s} + \mathbf{z})\mathbf{W}^\top + \mathbf{b} \\ &= (\widetilde{\mathbf{X}} \odot \mathbf{s})\mathbf{W}^\top + \mathbf{z}\mathbf{W}^\top + \mathbf{b} \\ &= \widetilde{\mathbf{X}}(\mathbf{W}^\top \odot \mathbf{s}^\top) + (\mathbf{z}\mathbf{W}^\top + \mathbf{b}). \end{aligned} \quad (3)$$

According to [Eq. \(3\)](#), weight and bias can absorb \mathbf{s} and \mathbf{z} , respectively, and thus becomes:

$$\begin{aligned} \widetilde{\mathbf{W}} &= \mathbf{W} \odot \begin{bmatrix} \mathbf{s}_1 & \mathbf{s}_2 & \dots & \mathbf{s}_n \\ \mathbf{s}_1 & \mathbf{s}_2 & \dots & \mathbf{s}_n \\ \dots & & & \\ \mathbf{s}_1 & \mathbf{s}_2 & \dots & \mathbf{s}_n \end{bmatrix}, \\ \widetilde{\mathbf{b}} &= \mathbf{z}\mathbf{W}^\top + \mathbf{b}. \end{aligned} \quad (4)$$

Take the typical challenging activation (output of LayerNorm) as an example here, [Fig. 2\(a\)](#) depicts that for attention structure, all following weights and biases can absorb the shifting and scaling signals without any extra computation burden.

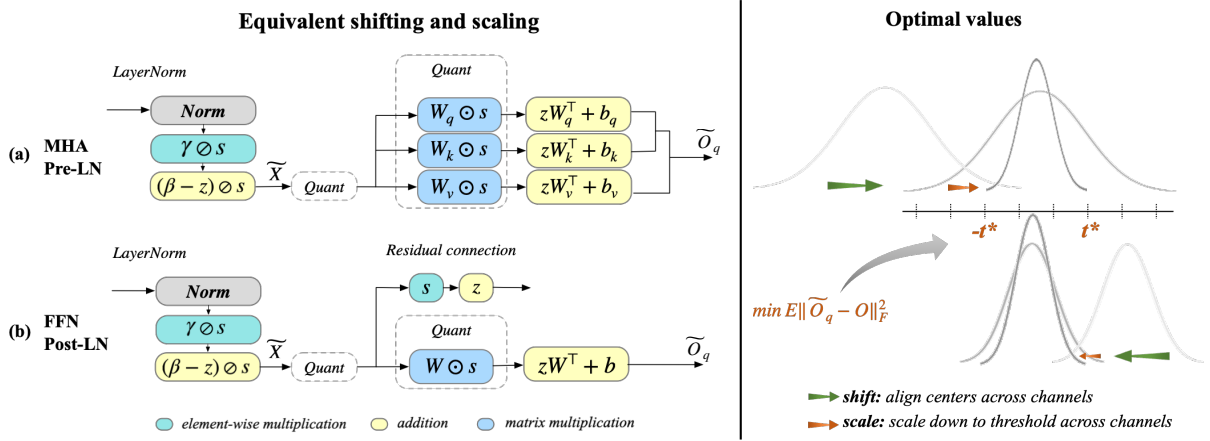


Figure 2: **Left:** We show the equivalent shifting and scaling operations by giving two representative examples: (a) for problematic output of Pre-LN (LayerNorm put inside residual connection) with Multi-Head Attention (MHA) structure; (b) for problematic output of Post-LN (LayerNorm put before residual connection) with Feed-Forward Network (FFN). **Right:** For optimal shifting and scaling values, the shifting vector can align the center of each channel to 0 and the scaling vector would shrink outliers into the outlier threshold t which is searched based on its left metric.

Residual connection. Second, we consider the case where a residual connection is applied after the LayerNorm structure (Post-LN) and fed into the quantized input. As shown in Fig. 2b, in addition to linear layer transformation, the identity function will be substituted with channel-wise multiplication and addition to maintain equivalence. We demonstrate that these increased calculations will only incur a negligible inference burden in Sec. 4.4.

Finally, because s and z serve as shared parameters across tokens and batches of data, the unified migration pattern can be implemented successfully and produce an equivalent FP model without additional computation most of the time.

3.2 Optimal shifting and scaling

Based on the equivalent shifting and scaling operations, in this section, we describe the way to efficiently and effectively obtain optimal solutions. An optimal shifting vector could solve the asymmetry of outliers while scaling factors further scale down outliers and bring marginal impact on the subsequent weights.

3.2.1 Shifting values

To eliminate the impact of asymmetry, we propose to align the center of each channel to 0 so that the range of the whole tensor reduces to the largest channel range (Fig. 1b, Fig. 2), getting rid of defined by asymmetric outliers. In this way, shifting values can be computed as the average of the minimum and maximum signals for each channel,

defined by:

$$z_j = \frac{\max(\mathbf{X}_{:,j}) + \min(\mathbf{X}_{:,j})}{2}. \quad (5)$$

3.2.2 Scaling factors

Challenges. Compared to shifting vectors, computing optimal scaling factors is more difficult because it also scales weight in the next layer, potentially leading to inferior weight quantization. Despite this, an appropriate scaling factor can still be useful because of the considerably narrower range weight holds (e.g., < 1 magnitude order) as opposed to activation with extreme outliers, making the enlargement of the weight range relatively small.

We propose optimizing scaling factors that adequately suppress activation outliers while not compromising weight quantization error to reach a balanced quantization burden. The following sections first explain the designed optimization objective and then describe the optimization procedure.

Optimization objective. When calculating a scaling vector, previous works (Wei et al., 2022b; Xiao et al., 2022) either ignore the affected following weight or simply equalize ranges of activation and weight. Unlike them, we think the key point is the involvement of scaled and quantized activation and weight in a neural network and introduce a loss-aware paradigm.

We first study the simple case that the problematic activation acts as the input of one linear layer (e.g., Fig. 2b). Instead of minimizing quantization errors of activation and weight separately (i.e., $\min_s \mathbb{E} [\|Q((\mathbf{X} - \mathbf{z}) \odot s) - (\mathbf{X} - \mathbf{z}) \odot s\|_F^2]$

and $\min_s \mathbb{E} [\|Q(\mathbf{W} \odot \mathbf{s}) - \mathbf{W} \odot \mathbf{s}\|_F^2]$, a task loss perspective is adopted by concerning their matrix multiplication output. We measure the output change after scaling and quantizing weight and activation to pursue optimal factors, given by:

$$\begin{aligned} \min_s \mathbb{E} [\| & \underbrace{Q((\mathbf{X} - \mathbf{z}) \odot \mathbf{s})Q(\mathbf{W} \odot \mathbf{s})^\top + \tilde{\mathbf{b}}}_{\text{output after scaling and quantization}} \\ & - (\mathbf{X}\mathbf{W}^\top + \mathbf{b}) \|_F^2], \\ & \underbrace{\text{original FP output}} \end{aligned} \quad (6)$$

where the mean squared error (MSE) is used to quantify the difference.

Multiple linear layers. Furthermore, we study the case where the troublesome activation becomes the input of multiple linear layers such as the attention structure (Fig. 2a).

In this scenario, three weights will be multiplied by the same scaling vector and calculated with the same suppressed activation. We mark the three outputs of matrix multiplication produced by scaled and quantized matrices as $\tilde{\mathbf{Q}}_q, \tilde{\mathbf{K}}_q, \tilde{\mathbf{V}}_q$, (Original outputs are denoted as $\mathbf{Q}, \mathbf{K}, \mathbf{V}$). Applying Eq. (6) to three linear layers separately and simply summing the losses can make it difficult to illustrate their different importance and usages. Therefore, we employ the attention mechanism as a post-process function to reasonably organize their scaling and quantization information as follows:

$$\min_s \mathbb{E} [\|\text{softmax}(\tilde{\mathbf{Q}}_q \tilde{\mathbf{K}}_q^\top) \tilde{\mathbf{V}}_q - \text{softmax}(\mathbf{Q} \mathbf{K}^\top) \mathbf{V}\|_F^2]. \quad (7)$$

Normalization and masking are omitted for notation simplicity. By applying Eq. (7), the change of the first two linear layers has been encapsulated within the attention map, bringing a more appropriate optimization objective for multiple linear layers.

Optimization procedure. We introduce an efficient and effective procedure to obtain the optimal scaling factors toward the above objective. First, we find that scaling down only channels with outliers can bring better performance. Because channels with normal activations can exhibit more variation over different inputs, it can be difficult to find a decent scaling value for them. Also, considering that they are not responsible for low quantization performance, scaling them is not necessary. Second, we propose to optimize an alternate variable called outlier threshold t , which would squeeze only channels with an activation range over t into

$(-t, t)$ and keep others intact (Fig. 2). Essentially, t here is used to specify which channel to scale down, the final scaled activation range, as well as the scaling values in the following weights.

This technique simplifies the complex problem with numerous variables \mathbf{s} to a single variable t . Then we can adopt the simple grid search for t to minimize the objective proposed in Eq. (6), Eq. (7). After getting the optimal t , the scaling vector is calculated as:

$$s_j = \max(1.0, \frac{\max(\mathbf{X}_{:,j} - \mathbf{z}_j)}{t}). \quad (8)$$

4 Experiments

The evaluations are designed to showcase: **I.** consistent and satisfactory predictions of the proposed approach for both small and large language models across different bit-widths and tasks; **II.** efficiency from both algorithm and deployment perspectives; and **III.** the efficacy of each component.

4.1 Set up

Models and tasks. We conduct experiments on both small and large language models. First, BERT models (base and large versions) are evaluated on the GLUE benchmark (Wang et al., 2018a), which consists of eight text classification tasks. Second, four of the largest OPTs ranging from 13B to 175B, along with the biggest BLOOM (Scao et al., 2022) and BLOOMZ (Muennighoff et al., 2022) boasting 176 billion parameters, are chosen as representatives. To verify the efficacy of our techniques on them, we adopt eight zero-short tasks (language modeling, multiple choice, commonsense reasoning, etc.) that can pose greater challenges for quantization. The evaluation code is based on lm-harness-evaluation¹.

Quantization setting. Quantization nodes are inserted as described in Wei et al. (2022b); NVIDIA (2022). Two types of quantization schemes are considered for static and standard quantization. The first is per-tensor and symmetric quantization, offering the fastest speed, indicated by an * (e.g., INT8*). The second is per-channel (weight) and asymmetric quantization, which provides high performance.

Notation: We use INT8 and INT6 to denote 8-bit and 6-bit activation and per-channel weight quantization, respectively. INT8* especially refers to per-tensor weight quantization. Activation always

¹<https://github.com/EleutherAI/lm-evaluation-harness>

employs per-tensor quantization. Additionally, ♣ marks those taking dynamic and fine-grained quantization schemes.

Implementation details. We randomly select 128 samples from the training dataset, in-domain data for the GLUE benchmark, and PILE (Gao et al., 2020) dataset for zero-shot tasks. A batch of them such as 32 is first used to calculate optimal shifting and scaling vectors. Then, we conduct the calibration procedure. Usually, MinMax calibration is employed but for models like BERT that also have a significantly varied token range, we apply the clipping method designed in Wei et al. (2022b). More details can be found in Appendix C. With our suppression framework, the transformed model can benefit from static quantization.

4.2 Small models

Baselines. The main baseline categories are described below:

MinMax obtains the minimum and maximum statistics of the tensor for quantization clipping range.

Percentile (Wu et al., 2020) uses the activation distribution percentile as the quantization clipping range. Using the dev set, we search its hyper-parameters within [0.999, 0.9999, 0.99999].

OMSE (Choukroun et al., 2019) minimizes the mean squared error between quantization and FP signals.

PEG (Bondarenko et al., 2021) applies fine-grained quantization to problematic activation from a channel perspective.

Outlier Suppression (OS) (Wei et al., 2022b) uses fixed scaling factors to suppress outliers and further clips outliers in a token-wise manner.

BERT. Table 1 gives prediction results of common post-training quantization algorithms. Most methods perform well on INT8* and INT8 but fail on lower bits while our approach consistently achieves superior outcomes. Compared to Wei et al. (2022b), our method outperforms by 1.6% and 15.5% on 6-bit and 4-bit, respectively. In summary, our approach can achieve near-floating point performance on high bits and reduce the performance gap to 5.6% on 4-bit.

4.3 Large language models

Baselines. The main baseline categories are described below.

ZeroQuant (Yao et al., 2022) uses per-token quantization, assigning different quantization parameters to different tokens. This fine-grained scheme from the token aspect also requires dynamic quantization. Meanwhile, for INT8*, we use per-group weight quantization according to its description.

Method	CoLA	MNLI	QNLI	SST-2	STS-B	Avg.
FP32	59.6	84.9	91.8	93.4	89.5	83.8
INT8*						
MinMax	52.3	81.3	89.0	91.1	86.2	79.5
OMSE	54.8	82.1	89.7	91.3	87.7	81.6
PEG	59.4	81.3	91.1	92.7	87.9	82.5
OS	60.3	83.9	90.2	92.9	88.2	83.0
Ours	60.9	84.4	91.1	92.7	88.3	83.5
INT6						
OMSE	35.4	73.7	84.7	86.3	85.8	73.5
Percentile	37.3	72.1	79.4	87.3	86.8	72.9
OS	54.4	81.8	89.8	91.9	88.7	81.2
Ours	56.0	84.5	90.9	92.4	89.5	82.8
INT4						
OMSE	4.7	38.5	52.2	50.3	0.2	41.1
Percentile	7.0	53.0	61.5	77.1	66.1	57.0
OS	28.5	57.9	72.5	80.4	67.8	62.7
Ours	50.0	80.2	85.4	91.4	86.5	78.2

Table 1: PTQ performance of BERT-base models. MNLI and STS-B report the combined score. **Avg.** indicates the averaged results of 8 tasks on GLUE benchmark (details in Appendix B). * means per-tensor quantization for weight. OS indicates Outlier Suppression for short.

LLM.int8() (Dettmers et al., 2022) employs per-token quantization and relaxes representation to FP16 for channels with signals greater than 6. The fine-grained and dynamic quantization scheme achieves favorable results but has a poorer latency performance. Thus, we only adopt its accuracy results as a superior target.

SmoothQuant (Xiao et al., 2022) migrates scaling factors to later modules to smooth problematic activation. Their scaling factors equal the range between activation and weights. For lower bits, we also search its hyper-parameter α according to its description for better performance.

OPTs. We list 8-bit and 6-bit quantization accuracy in Table 2. Our mechanism allows static and standard quantization to deliver comparable results to dynamic and fine-grained methods such as LLM.int8() that assigns FP16 for channels with signals over 6, and outperform ZeroQuant by a large margin. Meanwhile, while SmoothQuant suffers from non-negligible accuracy drops on much harder settings like 6-bit 175B model with significantly severe outliers, ours still gives enjoyable results, owning 28.3% upswings on StoryCloze task, 27.4% boost on PIQA. To conclude, ours is indeed close to FP results on 8-bit and exhibits around 1 point accuracy degradation on 6-bit.

BLOOM and BLOOMZ. Table 5 shows the performance on BLOOM and BLOOMZ with 176B parameters. It can be observed that their quantization challenges are less severe than OPTs with smaller accuracy drops across methods. And our approach still beats the best of others by about 2%

Name	Method	OPT-13B				OPT-30B				OPT-66B				OPT-175B				
		FP16	INT8*	INT8	INT6													
PIQA	LLM.int8()	-	75.8	-	-	-	77.3	-	-	-	78.7	-	-	-	79.6	-	-	
	ZeroQuant	75.8	54.1	-	53.0	77.6	54.2	-	52.0	78.7	53.2	-	51.9	79.7	52.3	-	53.1	
	SmoothQuant	-	-	73.5	-	77.2	-	66.7	-	78.3	-	52.0	-	79.7	-	52.6	-	
	Ours	76.4	75.9	75.8	-	77.4	77.6	77.4	-	78.7	78.6	77.5	-	79.6	79.5	80.0	-	
LAMBADA	LLM.int8()	-	68.4	-	-	-	71.4	-	-	-	73.8	-	-	-	74.6	-	-	
	ZeroQuant	68.6	0.0	-	0.0	71.5	0.0	-	0.0	73.9	0.0	-	0.0	74.7	0.0	-	0.0	
	SmoothQuant	-	68.3	-	65.2	-	71.0	-	13.4	-	72.9	-	0.0	-	74.6	-	0.5	
	Ours	68.3	68.4	65.7	-	70.8	70.8	69.6	-	73.0	73.4	72.7	-	74.5	74.5	74.2	-	
HellaSwag	LLM.int8()	-	52.4	-	-	-	54.3	-	-	-	56.3	-	-	-	59.2	-	-	
	ZeroQuant	52.5	26.5	-	25.8	54.3	26.4	-	25.7	56.4	26.1	-	25.7	59.3	25.4	-	25.6	
	SmoothQuant	-	52.2	-	49.2	-	54.2	-	37.4	-	55.9	-	26.5	-	58.9	-	26.0	
	Ours	52.3	52.5	51.7	-	54.2	54.2	53.7	-	56.2	56.3	55.8	-	59.2	59.3	58.5	-	
Winogrande	LLM.int8()	-	64.8	-	-	-	68.1	-	-	-	68.5	-	-	-	72.3	-	-	
	ZeroQuant	65.1	52.1	-	51.1	68.5	51.8	-	51.8	68.9	50.7	-	48.0	72.5	50.2	-	49.1	
	SmoothQuant	-	64.9	-	60.3	-	68.2	-	55.0	-	68.3	-	52.1	-	71.2	-	49.1	
	Ours	65.0	65.3	64.0	-	68.0	68.5	68.9	-	69.0	68.8	69.4	-	72.5	72.5	71.7	-	
(Challenge)	LLM.int8()	-	33.5	-	-	-	34.7	-	-	-	37.0	-	-	-	40.9	-	-	
	ZeroQuant	32.8	19.3	-	20.7	34.6	19.8	-	20.6	37.3	20.8	-	20.4	40.3	21.8	-	20.6	
	SmoothQuant	-	32.1	-	30.6	-	33.8	-	26.7	-	36.5	-	21.9	-	40.5	-	21.2	
	Ours	33.5	33.3	32.7	-	34.5	34.7	34.6	-	37.5	37.2	37.0	-	40.3	39.9	41.0	-	
(Easy)	LLM.int8()	-	67.3	-	-	-	69.7	-	-	-	71.8	-	-	-	74.8	-	-	
	ZeroQuant	67.3	27.5	-	25.0	70.1	30.5	-	25.0	71.7	29.7	-	26.0	74.9	24.0	-	25.6	
	SmoothQuant	-	66.2	-	62.2	-	69.7	-	55.8	-	70.5	-	27.8	-	74.1	-	28.8	
	Ours	67.3	66.8	67.0	-	70.1	70.0	68.9	-	71.3	71.8	70.7	-	74.8	74.7	74.3	-	
COPA	LLM.int8()	-	86.0	-	-	-	82.0	-	-	-	87.0	-	-	-	89.0	-	-	
	ZeroQuant	86.0	63.0	-	55.0	82.0	55.0	-	55.0	86.0	53.0	-	52.0	88.0	60.0	-	55.0	
	SmoothQuant	-	85.0	-	82.0	-	83.0	-	75.0	-	84.0	-	55.0	-	88.0	-	55.0	
	Ours	85.0	86.0	85.0	-	83.0	82.0	84.0	-	85.0	86.0	84.0	-	88.0	89.0	91.0	-	
StoryCloze	LLM.int8()	-	76.1	49.6	-	48.3	77.0	48.5	-	48.0	77.5	49.2	-	48.4	79.5	47.7	-	48.2
	ZeroQuant	-	76.0	-	73.5	-	76.9	-	61.4	-	77.3	-	48.8	-	79.1	-	49.8	
	SmoothQuant	-	75.8	76.0	75.4	-	77.0	76.9	76.6	-	77.3	76.4	76.6	-	79.2	79.1	78.1	-
	Ours	65.5	65.5	65.5	64.7	67.0	66.9	66.8	66.7	68.8	68.5	68.6	68.0	71.1	71.0	71.1	71.1	-

Table 2: Comparison among different techniques in terms of accuracy on eight zero-shot tasks. \clubsuit denotes dynamic quantization. Note that LLM.int8() would assign FP16 for channels containing signals over 6. INT8* specifically adopts per-tensor quantization for weights compared to INT8.

points on 6-bit.

4.4 Computational Complexity

In this part, we explain the computational complexity from algorithm and deployment aspects.

Algorithm efficiency. Our algorithm is efficient, able to generate scaling and shifting values in about 20 minutes for OPT-175B offline. Moreover, due to the equivalent transformation, our method does not demand additional training and can be applied in a post-training setting.

Deployment efficiency. Our method also en-

joys favorable speed improvements without extra computation burden for LLMs. For example, Fig. 3 demonstrates 1.50 \times acceleration on OPT-13B when compared to FP16. In most cases, the shifting and scaling operations can be seamlessly integrated into the subsequent modules. The only exception is the case of BERT models where the identity function in residual connection is replaced with channel-wise multiplication and addition to transform the activation back. Nevertheless, due to the limited presence of this structure, we demonstrate that these computations overhead are negligi-

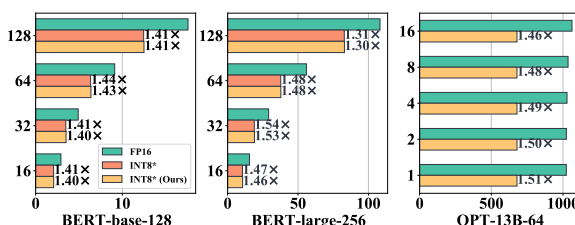


Figure 3: Real latency (x-axis) of our transformed 8-bit models, 8-bit and FP16 original models over different batch sizes (y-axis). BERT-large-256 refers to the BERT-large model with sequence length set to 256. Both numbers indicate quantization speedup. Only on BERT models, our transformation would increase the extra computation burden but is negligible.

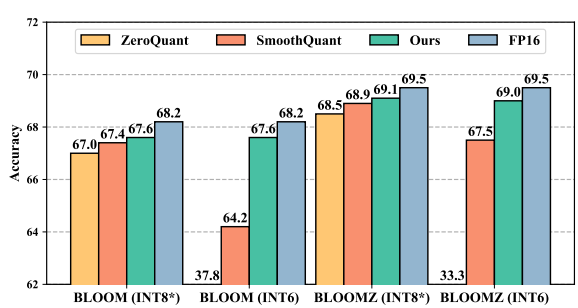


Figure 4: Averaged results of quantized BLOOM and BLOOMZ model on PIQA, Winogrande, LAMBADA, and HellaSwag. Detailed performance please see Appendix B.

Method	OPT-66B (INT6)		BERT (INT4)	
	PIQA	Winogrande	SST-2	MNLI
scaling	76.5	66.5	89.3	77.7
- attention post process	74.5	57.4	89.1	77.1
- outlier threshold	Fail	Fail	83.2	65.2

Table 3: Design choices of scaling factor. The second row removes the attention post process in optimization objective. The third row chooses to learn the scaling vector directly rather than alternately optimize the outlier threshold.

ble compared to normal INT8, as shown in Fig. 3.

4.5 Ablation study

Design choices of scaling factors. In this section, we compare different designs for the scaling vector. In Table 3, the second row illustrates the results without attention post-process Eq. (7). It is evident that simply summing the losses of multiple linear layers is not a wise choice, which suffers from significant performance declines: about 2% and 10% on OPTs and a smaller decline on BERT. The third row removes the outlier threshold and instead adopts learning scaling factors directly. We find this process is unstable and requires suitable hyperparameters, even causing failure on LLMs. Even though we perform the learning procedure carefully and report the best result for BERT, we still cannot obtain satisfying results. As mentioned in Sec. 3.2.2, this can be caused by poor scaling values for normal channels with varied signals.

Effect of each operation. From Table 4, it can be observed clearly that by removing the shifting operation, the accuracy drops by about 1%-3% under difficult settings. This is because, without channel-wise shifting that initially smooths the quantization challenge, scaling factors struggle to suppress outliers effectively while producing the tolerable weight quantization burden. Furthermore, when excluding scaling effects, performance decreases significantly, with even crashed results on LLMs.

4.6 Analysis of model storage and accuracy

Inspired by a variety of models with diverse sizes, we also study the relationship between their storage

Method	OPT-66B (INT6)		BERT (INT4)	
	PIQA	Winogrande	SST-2	MNLI
Ours	77.5	69.4	91.4	80.2
- shifting	76.5	66.5	89.3	77.7
- shifting - scaling	54.7	49.4	82.3	63.7

Table 4: Effect of scaling and shifting operations.

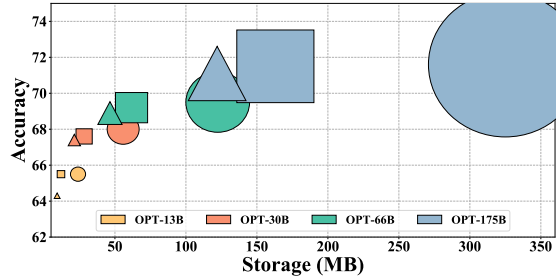


Figure 5: Averaged accuracy on PIQA, Winogrande, LAMBADA, and HellaSwag of OPTs with different storages. We draw circles, rectangles, and triangles to refer to FP16, the 8-bit and 6-bit models with quantized activation and weight.

and accuracy under quantization settings. Focusing on one kind of model with distinct quantization bit-width, Fig. 5 shows that 8-bit quantization which cuts storage by about half, can generally maintain original performance, and 6-bit quantization can lead to less performance drop on larger models. Moreover, considering fixed storage constraints, we discover that quantized big models typically outperform small FP models. These observations can relate to model robustness, which implies that large models can benefit from compression more if special outliers are handled well.

5 Conclusion and Limitations

We present the Outlier Suppression+ framework for addressing asymmetric and consistent outliers in LLMs and other transformers. Our framework is simple to use, consisting of both scaling and shifting operations, which can be efficiently and effectively implemented. Experiments demonstrate the efficacy of our methods for suppressing outliers. Below, we briefly discuss some limitations.

Other application scenarios: While we have applied our technique to language models under static and standard quantization, it is also interesting to explore vision scenario and the combination of our method with other quantization schemes like per-token quantization.

Deep level investigations: While we have observed features of outliers and devised methods to deal with them, the underlying reasons for their emergence and attributes have not been fully understood. This may require an in-depth analysis of the training pipeline, including the procedure and hyperparameters. Such investigations are time-consuming but can benefit both FP and quantized scenarios.

References

Haoli Bai, Wei Zhang, Lu Hou, Lifeng Shang, Jing Jin, Xin Jiang, Qun Liu, Michael Lyu, and Irwin King. 2020. Binarybert: Pushing the limit of bert quantization. *arXiv preprint arXiv:2012.15701*.

Ron Banner, Yury Nahshan, Elad Hoffer, and Daniel Soudry. 2018. Aciq: analytical clipping for integer quantization of neural networks.

Yelysei Bondarenko, Markus Nagel, and Tijmen Blankevoort. 2021. Understanding and overcoming the challenges of efficient transformer quantization. *arXiv preprint arXiv:2109.12948*.

Tom Brown, Benjamin Mann, Nick Ryder, Melanie Subbiah, Jared D Kaplan, Prafulla Dhariwal, Arvind Neelakantan, Pranav Shyam, Girish Sastry, Amanda Askell, et al. 2020. Language models are few-shot learners. *Advances in neural information processing systems*, 33:1877–1901.

Yaohui Cai, Zhewei Yao, Zhen Dong, Amir Gholami, Michael W Mahoney, and Kurt Keutzer. 2020. Zerorq: A novel zero shot quantization framework. In *Proceedings of the IEEE/CVF Conference on Computer Vision and Pattern Recognition*, pages 13169–13178.

Zhaowei Cai and Nuno Vasconcelos. 2020. Rethinking differentiable search for mixed-precision neural networks. In *Proceedings of the IEEE/CVF Conference on Computer Vision and Pattern Recognition*, pages 2349–2358.

Jungwook Choi, Zhuo Wang, Swagath Venkataramani, Pierce I-Jen Chuang, Vijayalakshmi Srinivasan, and Kailash Gopalakrishnan. 2018. Pact: Parameterized clipping activation for quantized neural networks. *arXiv preprint arXiv:1805.06085*.

Yoni Choukroun, Eli Kravchik, Fan Yang, and Pavel Kisilev. 2019. Low-bit quantization of neural networks for efficient inference. In *2019 IEEE/CVF International Conference on Computer Vision Workshop (ICCVW)*, pages 3009–3018. IEEE.

Matthieu Courbariaux, Yoshua Bengio, and Jean-Pierre David. 2015. Binaryconnect: Training deep neural networks with binary weights during propagations. *Advances in neural information processing systems*, 28.

Tim Dettmers, Mike Lewis, Younes Belkada, and Luke Zettlemoyer. 2022. Llm. int8 (): 8-bit matrix multiplication for transformers at scale. *arXiv preprint arXiv:2208.07339*.

Tim Dettmers and Luke Zettlemoyer. 2022. The case for 4-bit precision: k-bit inference scaling laws. *arXiv preprint arXiv:2212.09720*.

Jacob Devlin, Ming-Wei Chang, Kenton Lee, and Kristina Toutanova. 2018. Bert: Pre-training of deep bidirectional transformers for language understanding. *arXiv preprint arXiv:1810.04805*.

Zhen Dong, Zhewei Yao, Amir Gholami, Michael W Mahoney, and Kurt Keutzer. 2019. Hawq: Hessian aware quantization of neural networks with mixed-precision. In *Proceedings of the IEEE/CVF International Conference on Computer Vision*, pages 293–302.

Steven K Esser, Jeffrey L McKinstry, Deepika Bablani, Rathinakumar Appuswamy, and Dharmendra S Modha. 2019. Learned step size quantization. *arXiv preprint arXiv:1902.08153*.

Angela Fan, Pierre Stock, Benjamin Graham, Edouard Grave, Rémi Gribonval, Hervé Jegou, and Armand Joulin. 2020. Training with quantization noise for extreme model compression. *arXiv preprint arXiv:2004.07320*.

Elias Frantar, Saleh Ashkboos, Torsten Hoefler, and Dan Alistarh. 2022. Gptq: Accurate post-training quantization for generative pre-trained transformers. *arXiv preprint arXiv:2210.17323*.

Leo Gao, Stella Biderman, Sid Black, Laurence Golding, Travis Hoppe, Charles Foster, Jason Phang, Horace He, Anish Thite, Noa Nabeshima, et al. 2020. The pile: An 800gb dataset of diverse text for language modeling. *arXiv preprint arXiv:2101.00027*.

Ruihao Gong, Xianglong Liu, Shenghu Jiang, Tianxiang Li, Peng Hu, Jiazen Lin, Fengwei Yu, and Junjie Yan. 2019. Differentiable soft quantization: Bridging full-precision and low-bit neural networks. In *The IEEE International Conference on Computer Vision (ICCV)*.

Cong Guo, Yuxian Qiu, Jingwen Leng, Xiaotian Gao, Chen Zhang, Yunxin Liu, Fan Yang, Yuhao Zhu, and Minyi Guo. 2022. Squant: On-the-fly data-free quantization via diagonal hessian approximation. *arXiv preprint arXiv:2202.07471*.

Cong Guo, Jiaming Tang, Weiming Hu, Jingwen Leng, Chen Zhang, Fan Yang, Yunxin Liu, Minyi Guo, and Yuhao Zhu. 2023. Olive: Accelerating large language models via hardware-friendly outlier-victim pair quantization. *Matrix*, 17(4.2):7–1.

Song Han, Huizi Mao, and William J Dally. 2015. Deep compression: Compressing deep neural networks with pruning, trained quantization and huffman coding. *arXiv preprint arXiv:1510.00149*.

Geoffrey Hinton, Oriol Vinyals, and Jeff Dean. 2015. Distilling the knowledge in a neural network. *arXiv preprint arXiv:1503.02531*.

Itay Hubara, Yury Nahshan, Yair Hanani, Ron Banner, and Daniel Soudry. 2021. Accurate post training quantization with small calibration sets. In *International Conference on Machine Learning*, pages 4466–4475. PMLR.

Benoit Jacob, Skirmantas Kligys, Bo Chen, Menglong Zhu, Matthew Tang, Andrew Howard, Hartwig

Adam, and Dmitry Kalenichenko. 2018. Quantization and training of neural networks for efficient integer-arithmetic-only inference. In *Proceedings of the IEEE Conference on Computer Vision and Pattern Recognition (CVPR)*.

Qing Jin, Jian Ren, Richard Zhuang, Sumant Hanumante, Zhengang Li, Zhiyu Chen, Yanzhi Wang, Kaiyuan Yang, and Sergey Tulyakov. 2022. F8net: Fixed-point 8-bit only multiplication for network quantization. *arXiv preprint arXiv:2202.05239*.

Sehoon Kim, Amir Gholami, Zhewei Yao, Michael W Mahoney, and Kurt Keutzer. 2021. I-bert: Integer-only bert quantization. In *International conference on machine learning*, pages 5506–5518. PMLR.

Olga Kovaleva, Saurabh Kulshreshtha, Anna Rogers, and Anna Rumshisky. 2021. Bert busters: Outlier dimensions that disrupt transformers. *arXiv preprint arXiv:2105.06990*.

Andrey Kuzmin, Mart Van Baalen, Yuwei Ren, Markus Nagel, Jorn Peters, and Tijmen Blankevoort. 2022. Fp8 quantization: The power of the exponent. *arXiv preprint arXiv:2208.09225*.

Yann LeCun, John Denker, and Sara Solla. 1989. Optimal brain damage. *Advances in neural information processing systems*, 2.

Yanjing Li, Sheng Xu, Baochang Zhang, Xianbin Cao, Peng Gao, and Guodong Guo. 2022. Q-vit: Accurate and fully quantized low-bit vision transformer. *arXiv preprint arXiv:2210.06707*.

Yuhang Li, Xin Dong, and Wei Wang. 2019. Additive powers-of-two quantization: An efficient non-uniform discretization for neural networks. *arXiv preprint arXiv:1909.13144*.

Yuhang Li, Ruihao Gong, Xu Tan, Yang Yang, Peng Hu, Qi Zhang, Fengwei Yu, Wei Wang, and Shi Gu. 2021. **Brecq: Pushing the limit of post-training quantization by block reconstruction.** In *International Conference on Learning Representations*.

Yinhan Liu, Myle Ott, Naman Goyal, Jingfei Du, Mandar Joshi, Danqi Chen, Omer Levy, Mike Lewis, Luke Zettlemoyer, and Veselin Stoyanov. 2019. Roberta: A robustly optimized bert pretraining approach. *arXiv preprint arXiv:1907.11692*.

Paulius Micikevicius, Dusan Stosic, Neil Burgess, Marius Cornea, Pradeep Dubey, Richard Grisenthwaite, Sangwon Ha, Alexander Heinecke, Patrick Judd, John Kamalu, et al. 2022. Fp8 formats for deep learning. *arXiv preprint arXiv:2209.05433*.

Niklas Muennighoff, Thomas Wang, Lintang Sutawika, Adam Roberts, Stella Biderman, Teven Le Scao, M Saiful Bari, Sheng Shen, Zheng-Xin Yong, Hailey Schoelkopf, et al. 2022. Crosslingual generalization through multitask finetuning. *arXiv preprint arXiv:2211.01786*.

Markus Nagel, Rana Ali Amjad, Mart Van Baalen, Christos Louizos, and Tijmen Blankevoort. 2020. Up or down? adaptive rounding for post-training quantization. In *International Conference on Machine Learning*, pages 7197–7206. PMLR.

Markus Nagel, Mart van Baalen, Tijmen Blankevoort, and Max Welling. 2019. Data-free quantization through weight equalization and bias correction. In *Proceedings of the IEEE/CVF International Conference on Computer Vision*, pages 1325–1334.

NVIDIA. 2022. Faster transformer. <https://github.com/NVIDIA/FasterTransformer>.

Giovanni Puccetti, Anna Rogers, Aleksandr Drozd, and Felice Dell’Orletta. 2022. Outliers dimensions that disrupt transformers are driven by frequency. *arXiv preprint arXiv:2205.11380*.

Haotong Qin, Yifu Ding, Mingyuan Zhang, Qinghua Yan, Aishan Liu, Qingqing Dang, Ziwei Liu, and Xianglong Liu. 2022. Bibert: Accurate fully binarized bert. *arXiv preprint arXiv:2203.06390*.

Alec Radford, Karthik Narasimhan, Tim Salimans, Ilya Sutskever, et al. 2018. Improving language understanding by generative pre-training.

Teven Le Scao, Angela Fan, Christopher Akiki, Ellie Pavlick, Suzana Ilić, Daniel Hesslow, Roman Castagné, Alexandra Sasha Luccioni, François Yvon, Matthias Gallé, et al. 2022. Bloom: A 176b-parameter open-access multilingual language model. *arXiv preprint arXiv:2211.05100*.

Mingzhu Shen, Feng Liang, Ruihao Gong, Yuhang Li, Chuming Li, Chen Lin, Fengwei Yu, Junjie Yan, and Wanli Ouyang. 2021. Once quantization-aware training: High performance extremely low-bit architecture search. In *Proceedings of the IEEE/CVF International Conference on Computer Vision (ICCV)*, pages 5340–5349.

Sheng Shen, Zhen Dong, Jiayu Ye, Linjian Ma, Zhewei Yao, Amir Gholami, Michael W Mahoney, and Kurt Keutzer. 2020. Q-bert: Hessian based ultra low precision quantization of bert. In *Proceedings of the AAAI Conference on Artificial Intelligence*, volume 34, pages 8815–8821.

Shaden Smith, Mostafa Patwary, Brandon Norick, Patrick LeGresley, Samyam Rajbhandari, Jared Casper, Zhun Liu, Shrimai Prabhumoye, George Zerveas, Vijay Korthikanti, et al. 2022. Using deepspeed and megatron to train megatron-turing nlg 530b, a large-scale generative language model. *arXiv preprint arXiv:2201.11990*.

Chaofan Tao, Lu Hou, Wei Zhang, Lifeng Shang, Xin Jiang, Qun Liu, Ping Luo, and Ngai Wong. 2022. Compression of generative pre-trained language models via quantization. *arXiv preprint arXiv:2203.10705*.

Alex Wang, Amanpreet Singh, Julian Michael, Felix Hill, Omer Levy, and Samuel R Bowman. 2018a. Glue: A multi-task benchmark and analysis platform for natural language understanding. *arXiv preprint arXiv:1804.07461*.

Naigang Wang, Jungwook Choi, Daniel Brand, Chia-Yu Chen, and Kailash Gopalakrishnan. 2018b. Training deep neural networks with 8-bit floating point numbers. *Advances in neural information processing systems*, 31.

Peisong Wang, Qiang Chen, Xiangyu He, and Jian Cheng. 2020. Towards accurate post-training network quantization via bit-split and stitching. In *International Conference on Machine Learning*, pages 9847–9856. PMLR.

Xiuying Wei, Ruihao Gong, Yuhang Li, Xianglong Liu, and Fengwei Yu. 2022a. **Qdrop: Randomly dropping quantization for extremely low-bit post-training quantization**. In *International Conference on Learning Representations*.

Xiuying Wei, Yunchen Zhang, Xiangguo Zhang, Ruihao Gong, Shanghang Zhang, Qi Zhang, Fengwei Yu, and Xianglong Liu. 2022b. Outlier suppression: Pushing the limit of low-bit transformer language models. *arXiv preprint arXiv:2209.13325*.

Hao Wu, Patrick Judd, Xiaojie Zhang, Mikhail Isaev, and Paulius Micikevicius. 2020. Integer quantization for deep learning inference: Principles and empirical evaluation. *arXiv preprint arXiv:2004.09602*.

Guangxuan Xiao, Ji Lin, Mickael Seznec, Julien Demouth, and Song Han. 2022. Smoothquant: Accurate and efficient post-training quantization for large language models. *arXiv preprint arXiv:2211.10438*.

Zhewei Yao, Reza Yazdani Aminabadi, Minjia Zhang, Xiaoxia Wu, Conglong Li, and Yuxiong He. 2022. Zeroquant: Efficient and affordable post-training quantization for large-scale transformers. *arXiv preprint arXiv:2206.01861*.

Zhihang Yuan, Chenhao Xue, Yiqi Chen, Qiang Wu, and Guangyu Sun. 2021. Ptq4vit: Post-training quantization framework for vision transformers. *arXiv preprint arXiv:2111.12293*.

Ofir Zafir, Guy Boudoukh, Peter Izsak, and Moshe Wasserblat. 2019. Q8bert: Quantized 8bit bert. In *2019 Fifth Workshop on Energy Efficient Machine Learning and Cognitive Computing-NeurIPS Edition (EMC2-NIPS)*, pages 36–39. IEEE.

Aohan Zeng, Xiao Liu, Zhengxiao Du, Zihan Wang, Hanyu Lai, Ming Ding, Zhuoyi Yang, Yifan Xu, Wendi Zheng, Xiao Xia, et al. 2022. Glm-130b: An open bilingual pre-trained model. *arXiv preprint arXiv:2210.02414*.

Dongqing Zhang, Jiaolong Yang, Dongqiangzi Ye, and Gang Hua. 2018. Lq-nets: Learned quantization for highly accurate and compact deep neural networks. In *Proceedings of the European conference on computer vision (ECCV)*, pages 365–382.

Susan Zhang, Stephen Roller, Naman Goyal, Mikel Artetxe, Moya Chen, Shuhui Chen, Christopher DeWan, Mona Diab, Xian Li, Xi Victoria Lin, et al. 2022. Opt: Open pre-trained transformer language models. *arXiv preprint arXiv:2205.01068*.

Wei Zhang, Lu Hou, Yichun Yin, Lifeng Shang, Xiao Chen, Xin Jiang, and Qun Liu. 2020. Ternarybert: Distillation-aware ultra-low bit bert. *arXiv preprint arXiv:2009.12812*.

Xiangguo Zhang, Haotong Qin, Yifu Ding, Ruihao Gong, Qinghua Yan, Renshuai Tao, Yuhang Li, Fengwei Yu, and Xianglong Liu. 2021. Diversifying sample generation for accurate data-free quantization. In *The IEEE Conference on Computer Vision and Pattern Recognition (CVPR)*.

Ritchie Zhao, Yuwei Hu, Jordan Dotzel, Chris De Sa, and Zhiru Zhang. 2019. Improving neural network quantization without retraining using outlier channel splitting. In *International conference on machine learning*, pages 7543–7552. PMLR.

Barret Zoph and Quoc V Le. 2016. Neural architecture search with reinforcement learning. *arXiv preprint arXiv:1611.01578*.

A Related work

Quantization. Quantization (Jacob et al., 2018) employs low-bit representations for activation and weight in neural networks. Researchers categorize this approach into two pipelines: post-training quantization (PTQ) and quantization-aware training (QAT). QAT (Courbariaux et al., 2015; Choi et al., 2018; Esser et al., 2019; Li et al., 2019; Gong et al., 2019; Shen et al., 2021; Zhang et al., 2018) trains the quantized model end-to-end, necessitating significant GPU resources and the entire training dataset. In contrast, PTQ (Choukroun et al., 2019; Wu et al., 2020; Banner et al., 2018; Wang et al., 2020; Zhao et al., 2019; Nagel et al., 2019) only requires hundreds of samples and limited resource consumption, producing a calibrated model quickly. Recently, several works (Nagel et al., 2020; Hubara et al., 2021; Li et al., 2021; Wei et al., 2022a) proposed to adjust models slightly for improved PTQ performance. Besides, other types of quantization include zero-shot quantization without real calibration data (Cai et al., 2020; Zhang et al., 2021; Guo et al., 2022), mixed-precision with mixed bit-width (Dong et al., 2019; Cai and Vasconcelos, 2020), and FP8 data type (Wang et al., 2018b; Kuzmin et al., 2022; Micikevicius et al., 2022; Jin et al., 2022).

Quantization of transformer language models. Recently, there has been a growing interest in the quantization of transformer language models. In the context of QAT, Zafrir et al. (2019) first explores 8-bit quantization for BERT-like models. Shen et al. (2020) introduces group-wise quantization and studies mixed-precision quantization based on Hessian information. Bai et al. (2020); Zhang et al. (2020); Qin et al. (2022) combine distillation strategies with quantization. Kim et al. (2021) approximates the nonlinear function in transformer architectures to enable integer-only inference. Fan et al. (2020) incorporates quantization noise for enhancement. Additionally, Tao et al. (2022) investigates the challenges of quantizing generative models.

In the realm of PTQ, researchers have discovered that the poor performance of these models should be attributed to extreme outliers in activations. These outliers exhibit special characteristics from both channel and token aspects. *In terms of channels*, outliers consistently emerge in certain channels over different inputs. Bondarenko et al. (2021) employs a per-embedding-group quantiza-

tion scheme that uses different quantization parameters for distinct channel groups, while Dettmers et al. (2022) suggests utilizing FP16 representations for problematic channels holding signals over 6. Wei et al. (2022b) identifies this feature lying in LayerNorm’s output and migrates the scaling parameter of LayerNorm to subsequent modules to attenuate outliers. Xiao et al. (2022) proposes calculating scaling values by equalizing ranges between activations and weights. Guo et al. (2023) discards normal values adjacent to outliers, making room for outliers with customized GPU support. Compared to them, we design the scaling factors that concern the interactive results of troublesome activation and following weights to scale down channels with outliers offline. Also, we notice the asymmetric presentation of outliers and design a shifting operation. *In terms of tokens*, different tokens exhibit varying degrees of outliers. Dettmers et al. (2022); Yao et al. (2022) introduce a novel scheme called per-token quantization that dynamically computes quantization parameters for each token. Wei et al. (2022b) investigates the clipping impact of outliers and recommends finding an appropriate clipping range in a token-wise manner.

Besides, some studies focus on weight quantization, such as Dettmers and Zettlemoyer (2022); Frantar et al. (2022); Zeng et al. (2022) and some including Yuan et al. (2021); Li et al. (2022), investigate the quantization of Vision Transformer (ViT) models. Interestingly, several studies (Kovaleva et al., 2021; Puccetti et al., 2022) explores the underlying reasons for emerging outliers and trace them back to the pre-training phase, shedding light on potential advancements in the field.

B Supplementary experiments

BERT-base. We provide detailed results of BERT-base models on GLUE benchmarks in Table 6. Interestingly, we find that models which are sensitive to different learning hyperparameters during the fine-tuning phase, such as CoLA and RTE, also exhibit less favorable quantization outcomes. This suggests a possible relationship between quantization and robustness.

BERT-large. We also conduct experiments on BERT-large models in Table 7. Results across methods indicate that quantizing BERT-large models is more challenging (e.g., MinMax suffers from a considerable accuracy drop (about 13%) on INT8* compared to BERT-base, and Outlier Suppression

Algorithm 1: Outlier Suppression+

Input: Problematic output \mathbf{X} of LayerNorm with parameters γ, β , subsequent module M with weight \mathbf{W} and bias \mathbf{b} , grid search iteration K .

{1. Optimal shifting and scaling:}

$$\mathbf{z} = \frac{\min(\mathbf{X}_{:,j}) + \max(\mathbf{X}_{:,j})}{2} \quad \triangleright \text{Optimal shifting vector.}$$
$$\text{loss}^* = \text{INF}$$

for $k = 1$ to K **do**

$$t = \max(\mathbf{X} - \mathbf{z}) \cdot \frac{k}{K}, \quad \triangleright \text{Enumerate outlier threshold.}$$
$$s_j = \max(1.0, \frac{\max(\mathbf{X}_{:,j} - \mathbf{z}_j)}{t})$$

Calculate loss_k based on Eq. (6), Eq. (7).

if $\text{loss}^* > \text{loss}_k$ **then**

$$|\text{loss}^* = \text{loss}_k, s^* = s \quad \triangleright \text{Optimal scaling factors.}$$

{2. Equivalent shifting and scaling:}

$$\tilde{\beta} = (\beta - \mathbf{z}) \oslash s^*, \tilde{\gamma} = \gamma \oslash s^* \quad \triangleright \text{Fuse } \mathbf{z}, s^* \text{ into former operations.}$$
$$\tilde{\mathbf{b}} = \mathbf{z}\mathbf{W}^\top + \mathbf{b}, \tilde{\mathbf{W}} = \mathbf{W} \odot s^* \quad \triangleright \text{Update following modules.}$$

return Transformed LayerNorm and subsequent module;

also fails on the 6-bit setting). Fortunately, with Outlier Suppression+, the results can be improved, yielding an 18.7% enhancement.

BLOOM and BLOOMZ. Here, we provide detailed results of different techniques for BLOOM and BLOOMZ in Table 5. Although SmoothQuant outperforms us on LAMBADA, we argue that it could be due to the instability of the dataset since it is already higher than FP results.

C Implementation details

In this section, we provide detailed descriptions of our implementation with the core part distilled in algorithm 1. Note that the mechanism is applied under a standard and static post-training quantization scenario, without any calibration calculation during the inference phase.

BERT. On the GLUE benchmark, fine-tuned FP models are used for quantization. We randomly se-

lect 128 samples and set the batch size to 32. First, a batch of data is used to calculate the optimal shifting and scaling signals for problematic activations, especially outputs after LayerNorm here. Then shifting and scaling vectors are fused into former operations and absorbed in later modules. On fused models, we apply the calibration procedure. Particularly, on BERT models, due to the great variance of token range as discussed in Yao et al. (2022); Wei et al. (2022b), we incorporate the Token-Wise Clipping proposed in Outlier Suppression which is an orthogonal technique and weakens outliers from the token aspect.

OPTs. For OPTs, we quantize pre-trained models and evaluate them on zero-shot tasks. 128 samples with sequence length set to 512 are randomly extracted from one of the train datasets, namely the PILE dataset. As we have observed that LayerNorm produces severe asymmetric outliers on certain channels, the proposed method is applied here. After obtaining a more quantization-friendly model, the MinMax algorithm collects distribution statistics. Since diverse tokens do not have outliers of varying degrees on these models, advanced clipping techniques are not involved.

BLOOM and BLOOMZ. The main pipeline is similar to OPTs. The only exception is using the Token-Wise Clipping as the calibration method because these models hold different outliers among different tokens. The clipping ratios are searched as 0.5% and 1.5% for 8-bit and 6-bit BLOOM, and 0.0% and 0.5% on BLOOMZ.

Method	Bits	HellaSwag	LAMBADA	PIQA	Winogrande
BLOOM-176B	FP16	55.9	67.7	78.8	70.3
ZeroQuant*	INT8*	54.8	67.8	76.0	69.4
SmoothQuant	INT8*	54.1	69.2	77.7	68.6
Ours	INT8*	54.9	68.0	78.4	69.1
ZeroQuant*	INT6	30.5	7.5	61.2	52.0
SmoothQuant	INT6	52.1	60.2	76.7	67.6
Ours	INT6	55.1	69.1	78.1	68.1
BLOOMZ-176B	FP16	57.1	67.8	80.6	72.5
ZeroQuant*	INT8*	56.3	67.6	79.1	70.9
SmoothQuant	INT8*	56.3	68.7	79.7	70.8
Ours	INT8*	56.7	68.5	79.9	71.3
ZeroQuant*	INT6	28.2	1.4	54.0	49.6
SmoothQuant	INT6	55.0	65.2	80.0	69.9
Ours	INT6	56.2	69.2	79.9	70.6

Table 5: Quantization results on 4 zero-shot tasks in terms of accuracy.

Method	CoLA (Matt.)	MNLI (acc m/mm)	MRPC (f1/acc)	QNLI (acc)	QQP (f1/acc)	RTE (acc)	SST-2 (acc)	STS-B (Pear./Spear.)	Avg.
FP32	59.6	84.9/84.8	91.4/87.8	91.8	87.8/90.9	72.6	93.4	89.7/89.3	83.8
INT8*									
MinMax	52.3	80.9/81.7	85.3/80.9	89.0	84.8/88.6	68.2	91.1	84.7/87.6	79.5
OMSE	54.8	81.9/82.2	89.7/86.0	89.7	86.1/89.5	72.2	91.3	87.2/88.2	81.6
PEG	59.4	81.3	88.5	91.1	89.4	69.3	92.7	87.9	82.5
OS	60.3	83.8/84.0	90.4/87.0	90.2	87.3/90.4	71.1	92.9	87.8/88.7	83.0
Ours	60.9	84.4/84.4	90.6/87.2	91.1	87.1/90.6	73.3	92.7	87.7/88.9	83.5
INT8									
MinMax	57.1	82.8/83.5	89.9/85.8	90.8	87.8/90.7	69.7	92.8	86.8/88.6	82.3
OMSE	57.2	84.0/84.3	90.1/85.8	91.1	87.6/90.5	72.2	92.2	87.9/88.7	82.9
Percentile	57.1	83.9/84.1	90.7/86.7	91.3	87.7/90.7	71.1	93.4	87.7/88.7	82.9
OS	61.6	84.4/84.5	91.4/87.8	91.5	87.9/90.8	72.2	93.8	89.2/89.0	84.0
Ours	60.3	84.8/84.5	90.5/87.0	91.6	87.5/90.8	71.5	93.6	89.3/89.2	83.6
INT6									
MinMax	17.7	32.5/32.5	0.7/31.9	65.2	40.9/69.0	48.0	82.0	59.8/60.3	47.1
OMSE	35.4	74.0/73.3	81.5/76.5	84.7	76.1/82.1	64.3	86.3	85.6/86.1	73.5
Percentile	37.3	72.4/71.7	85.1/79.9	79.4	72.6/80.2	61.7	87.3	86.4/87.3	72.9
OS	54.4	82.0/81.7	87.5/83.3	89.8	84.7/88.9	70.8	91.9	88.7/88.6	81.2
Ours	56.0	84.6/84.4	90.0/86.3	90.9	87.0/90.5	71.8	92.4	89.6/89.4	82.8
INT4									
MinMax	-6.6	32.6/32.7	0.0/31.6	50.6	53.8/36.8	47.7	50.9	-0.5/-0.5	29.5
OMSE	4.7	38.5/38.4	81.3/69.1	52.2	45.2/50.9	59.9	50.3	0.1/-0.4	41.1
Percentile	7.0	52.6/53.5	83.0/75.7	61.5	44.7/68.3	55.6	77.1	65.9/66.3	57.0
OS	28.5	57.5/58.3	83.9/75.7	72.5	45.4/70.8	56.7	80.4	67.8/67.9	62.7
Ours	50.0	80.6/79.9	87.6/83.1	85.4	85.0/77.5	65.7	91.4	86.4/86.5	78.2

Table 6: PTQ performance of BERT-base models on GLUE benchmark. * means per-tensor quantization for weight. OS indicates Outlier Suppression for short.

Method	CoLA (Matt.)	MNLI (acc m/mm)	MRPC (f1/acc)	QNLI (acc)	QQP (f1/acc)	RTE (acc)	SST-2 (acc)	STS-B (Pear./Spear.)	Avg.
FP32	63.3	86.7/85.9	91.6/88.0	92.2	88.1/91.1	74.0	93.5	90.3/90.1	84.9
INT8*									
MinMax	62.4	72.0/73.0	76.3/72.8	87.0	66.5/80.4	46.9	92.2	58.6/52.1	71.5
OMSE	59.9	82.7/83.5	87.8/83.8	89.0	79.2/86.2	47.3	92.0	83.9/83.3	78.1
Percentile	61.3	84.5/84.0	91.6/88.9	91.6	85.9/89.4	69.3	92.4	88.3/88.1	83.1
OS	62.3	85.1/84.5	90.1/86.0	91.1	87.0/90.3	75.1	92.4	88.7/88.4	83.9
Ours	62.2	85.9/85.2	90.9/87.0	92.2	87.8/90.8	71.8	93.3	89.3/89.3	84.1
INT6									
MinMax	5.6	32.0/32.0	50.2/46.1	50.2	0.0/63.2	49.5	53.0	5.0/4.8	38.1
OMSE	14.0	59.3/58.4	86.1/78.7	79.5	52.5/73.5	54.9	74.8	44.0/37.9	59.8
Percentile	16.4	63.5/63.8	82.0/77.2	87.0	44.8/70.7	49.8	81.7	65.7/67.8	62.8
OS	24.1	71.3/71.7	85.5/79.4	80.8	68.8/78.3	47.3	82.3	61.1/62.0	65.4
Ours	60.9	86.3/85.4	91.8/88.2	92.0	87.7/90.8	71.5	93.7	86.7/85.6	83.7

Table 7: PTQ performance of BERT-large models on GLUE benchmark. * means per-tensor quantization for weight. OS indicates Outlier Suppression for short.